Physics of Plasmas ARTICLE scitation.org/journal/php

Gyrokinetic analysis of inter-edge localized mode transport mechanisms in a DIII-D pedestal

Cite as: Phys. Plasmas **29**, 112505 (2022); doi: 10.1063/5.0102152
Submitted: 7 June 2022 · Accepted: 15 October 2022 ·
Published Online: 8 November 2022

M. R. Halfmoon,[1,a)] D. R. Hatch,[1] M. T. Kotschenreuther,[1] S. M. Mahajan,[1] A. O. Nelson,[2] E. Kolemen,[3] M. Curie,[4] A. Diallo,[3] R. J. Groebner,[4] E. Hassan,[5,6] E. A. Belli,[4] and J. Candy[4]

AFFILIATIONS

[1]Institute for Fusion Studies, University of Texas at Austin, Austin, Texas 78712, USA
[2]Columbia University, New York, New York 10027, USA
[3]Princeton Plasma Physics Lab, Princeton University, Princeton, New Jersey 08536, USA
[4]General Atomics, San Diego, California 92121, USA
[5]Oak Ridge National Laboratory, Oak Ridge, Tennessee 37830, USA
[6]Physics, Faculty of Science, Ain Shams University, Cairo 11566, Egypt

Note: This paper is part of the Special Topic: Papers from the 2022 Sherwood Fusion Theory Conference.
[a)]**Author to whom correspondence should be addressed:** michael.halfmoon@science.doe.gov

ABSTRACT

In this study, gyrokinetic simulations are used to study pedestal fluctuations for DIII-D discharge 174082 using the GENE code. Nonlinear local simulations indicate that electron heat flux has contributions from electron temperature gradient-driven transport but at levels insufficient to satisfy power balance. We show that microtearing modes (MTM) and neoclassical transport are likely to account for the remaining observed energy losses in the electron and ion channels, respectively. The MTM instabilities found in the simulations are consistent with the high-frequency fluctuations identified in the magnetic fluctuation data from Mirnov coils. The fluctuation data in this discharge also exhibit a low-frequency band of fluctuations. By modifying the equilibrium profiles and plasma β, simulations produce MHD modes, which may be responsible for these observed low-frequency fluctuations. We compare several metrics involving ratios of fluctuation amplitudes and transport quantities for both MTMs and MHD modes. This analysis suggests that the available data are consistent with the simultaneous activity of both MHD modes and MTMs provided that the former is limited largely to the particle transport channel.

I. INTRODUCTION

The edge transport barrier (ETB), or pedestal, is a thin region in an H-mode plasma that is characterized by inhibited transport[1] due to the suppression of the deleterious combination of ion temperature gradient (ITG) and trapped electron mode (TEM) instabilities. The formation of a pedestal with sufficiently high temperature will be a requirement for the success of ITER.

Several instabilities have emerged as viable candidates for the mechanisms behind observed anomalous density and energy transport in pedestals.[2] These instabilities include electron temperature gradient (ETG) modes,[3–7] kinetic ballooning modes (KBMs),[8–11] and microtearing modes (MTMs),[5,10,12–17] along with the possibility of residual ITG[6,7,18]/TEM[19] fluctuations. Gyrokinetic simulations predict that the transport from these micro-instabilities along with neoclassical transport can often be combined to account for observed transport levels within experimental uncertainties.[5,7,18–25]

Several studies have examined magnetic fluctuations in the pedestal region via external Mirnov coils.[26,27] Recently, studies have indicated that the MTM is the cause of prominent magnetic fluctuations observed in magnetic spectrograms[2,22,28–31] and a major source of inter-edge localized mode (ELM) electron heat transport in the steep gradient region of the pedestal.[2,5,6,31–36] Figure 1 is a magnetic spectrogram of DIII-D shot 174082, with strong fluctuations at the ≈100 and ≈400 kHz regions (circled in green) and low-frequency (≈50 kHz) magnetic "chatter" (circled in black).

Recent advances in experimental diagnostics on DIII-D have provided internal magnetic fluctuation data via a radial interferometer–polarimeter.[28,29] This technique provides line-integrated calculations

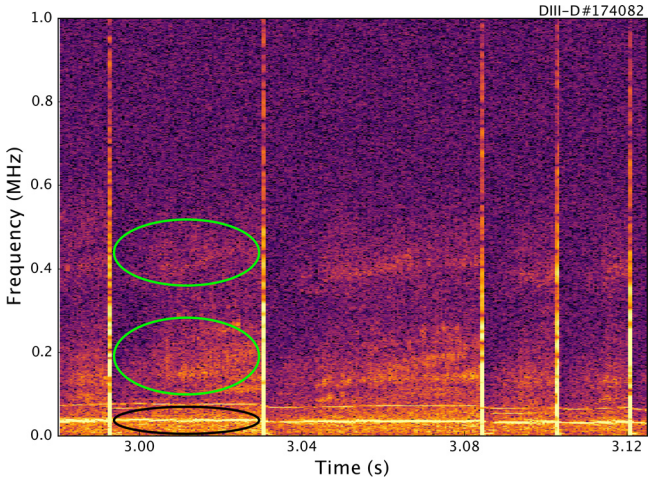

FIG. 1. Fast magnetics of shot 174082. Fluctuations at 0.1 and 0.4 MHz (circled in green) are found across each inter-ELM period. There is also a very low-frequency region of activity <0.05MHz (circled in black).

of magnetic fluctuations across a chord of the plasma, instead of the traditional technique via external pickup coils.[37] This tool allows for a more direct comparison with gyrokinetic simulations. An initial comparison along these lines will be reported in Ref. 32.

Given this evidence in favor of MTM as a major pedestal transport mechanism, an outstanding question is the role played by the KBM, which is proposed by the EPED model as the salient inter-ELM transport mechanism limiting the pedestal pressure profile.[38] In this paper, we consider both MTM and MHD-like modes (such as KBM) as contributors to pedestal transport and the observed magnetic fluctuations.

To this end, we analyze DIII-D shot 174082. In DIII-D discharge 174082, magnetic fluctuation diagnostics produce data that can be clearly identified as MTMs. Specifically, the measured signals between ~120 and ~420 kHz in shot 174082 align well with predicted values for MTMs with the equilibrium profiles under consideration, estimating the electron diamagnetic frequency using the formula $\omega_{e*} = k_y \rho_s c_s (1/L_{T_e} + 1/L_n)$, where the electron temperature and density gradient scale lengths are L_{T_e,n_e}, respectively, ρ_s is the ion gyroradius, c_s is the plasma sound speed, and k_y is the binormal wavenumber. We demonstrate this correspondence directly with simulations using the gyrokinetic code GENE.[3,39] The experimentally observed frequencies match closely the values identified in our gyrokinetic simulations of MTMs, with global simulations indicating that the MTM is the fastest growing mode.

We also carry out several numerical and thought experiments to probe the possible role of MHD modes. By modifying the equilibrium beta, simulations show that an MHD instability can become the fastest growing global linear mode. These simulations exhibit significantly higher transport ratios for normalized particle flux than MTMs and have ion-diamagnetic-directed frequencies. They also have frequencies in the range of the low-frequency activity observed in magnetic spectrograms for this discharge.

We compare several metrics involving ratios of fluctuation amplitudes and transport quantities for both MTMs and MHD modes. This analysis suggests that the available data are consistent with the simultaneous activity of both MHD modes and MTMs provided that the former is limited largely to the particle transport channel. This is the first time gyrokinetic analysis has been carried out for MTMs and MHD modes finding experimental signatures (notably, frequencies in the magnetic spectrogram) of both in the same discharge.

This paper is outlined as follows: First, the details of the experimental configuration under investigation will be discussed in Sec. II, with emphasis on the methodology of reconstructing profile data. Second, the gyrokinetic simulations performed using these experimental profiles will be laid out in detail in Sec. III, including the results of local linear scans in collisionality and wavenumber, global linear wavenumber scans, and local nonlinear simulations at the peak in ω_e^*. Third, simulation results will be compared with experimental transport and fluctuation measurements in Sec. IV.

II. EXPERIMENTAL PROFILES AND EQUILIBRIUM

The simulation of anomalous transport in pedestals requires profiles of temperature and density for all relevant particle species, the radial electric field, and a kinetic reconstruction of the magnetic equilibrium. To ensure that all of these effects are accurately obtained from the experimental discharge, extensive work has been performed using experimental diagnostics and modules found in the software suite OMFIT.[40] Kinetic equilibria were calculated manually from inter-ELM-averaged profiles and compared with the results from the CAKE code,[41] which provides self-consistent kinetic equilibria from automatic profile fitting and the EFIT Grad–Shafranov solver.[42] All profiles used in this study were then mapped onto the resulting kinetic equilibria. This study focuses on the baseline (174082) equilibrium from a study on the effects of pellet fueling on a neutral beam-heated plasma.[42] This shot is heated entirely by neutral beams at a rate of 4.67 MW, with no pellet injection involved. The resulting magnetic geometry and plasma profiles give snapshots of the DIII-D experiment.

This work utilizes the resulting magnetic geometry and profile data as input for the gyrokinetic solver GENE[39] to simulate the inter-ELM pedestal micro-instabilities. To account for the stiffness of the transport mechanisms, sensitivity tests are performed with changes to local equilibrium gradients that fall within the tolerance of these reconstructions. Overall, these equilibria are accurate representations of the inter-ELM steady state for a given shot due to systematic reconstruction via CAKE/EFIT, and thus, the resulting gyrokinetic simulations are performed with experimental inputs that are as accurate and comprehensive as possible.

Figure 2 depicts the density and temperature profiles across the pedestal region. Ion temperature is calculated using charge exchange recombination (CER) to find carbon temperature, carbon is treated as the dominant impurity species in simulations, and $T_i = T_C$. The radial electric field, E_r/RB_θ, is shown in Fig. 3. The magnetic geometry, pressure profile, and q-profile are shown in Fig. 4.

III. NUMERICAL INVESTIGATIONS

Advances in gyrokinetic codes have enabled accurate simulations of turbulence in fusion plasmas, matching experimental fluxes to an unprecedented degree. This is particularly true in the core plasma, where gyrokinetic orderings are more strictly satisfied and profile gradients are less extreme than in the pedestal.[40,44–53] Recently, simulations in the pedestal also demonstrate increasing correspondence with experimental trends and observations of transport and fluctuations.[5–7,18–20,22,24,54]

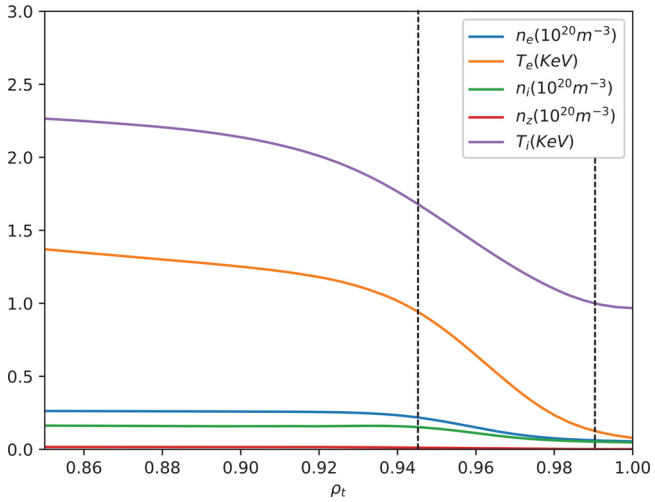

FIG. 2. Density and temperature profiles of the pedestal in baseline shot 174082. Global simulations extend from ρ_{tor} of 0.945 to 0.995, highlighted by the black dashed lines.

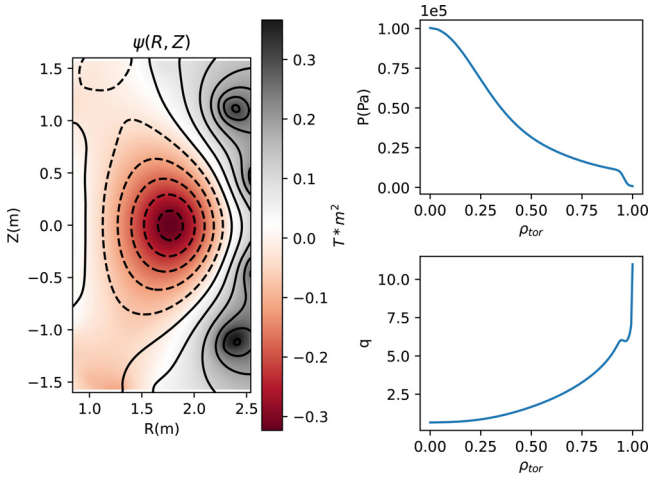

FIG. 4. EFIT profiles of DIII-D shot 174082. Noting the local minimum of the q-profile in the pedestal region, previous studies have found a link between low values of magnetic shear, $s = \frac{r}{q}\frac{dq}{dr}$, and a drive to the microtearing mode.[2,55]

The focus of this study is in the region of strongest electron temperature and density gradients near the plasma edge ($\rho = 0.945$–0.99) in order to identify the mechanisms that mediate pedestal development during the inter-ELM cycle and, thus, contribute to the ultimate pre-ELM pedestal structure.

A. Linear simulations

To gain insight into the driving mechanisms of observed turbulent fluctuations, a series of simulations using the gyrokinetic code GENE[3,39] was run based on the experimental scenario described above, scanning across a wide range of toroidal mode numbers. We consider both local and global simulations. Local linear simulations are performed at $\rho_{tor} = 0.965$ where ω_* peaks, as this corresponds

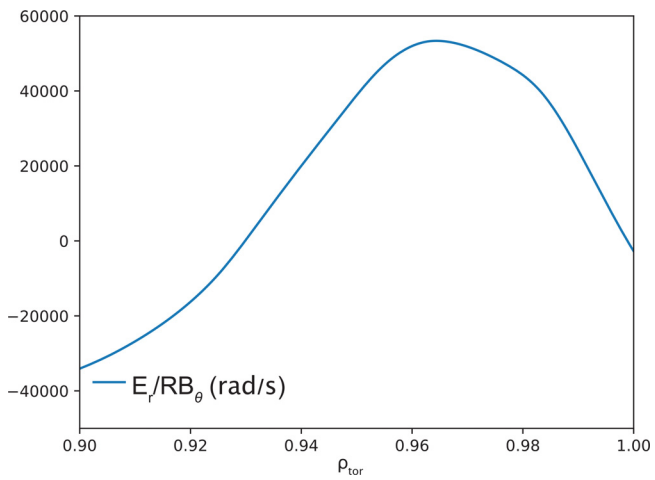

FIG. 3. E_r/RB_θ[43] velocity profile for shot 174082. This profile is utilized in all global GENE simulations.

most closely to the frequency observed in global simulations and has been shown elsewhere to be the location at which MTMs peak.[22,31,56] For typical local simulations, a resolution of $(k_x, z, v_\parallel, \mu) = (12, 96, 45, 24)$ is used (where k_x is the radial wavenumber, z is the real coordinate along the field line, and $v_\parallel$ and $v_\perp$ are the velocities relative to the field line), while global calculations require $(\rho_{tor}, z, v_\parallel, \mu) = (128, 96, 32, 16)$. Global simulations made use of the block structured grids feature in GENE,[57,58] allowing for lower resolutions in velocity space by resizing the velocity space domain to match the background temperature.

In Refs. 22, 31, 59, and 62, the alignment of mode-rational surfaces with the peak of the ω_{*e} profile was shown to be crucial for low-n MTM instability. This is an intrinsically global effect. However, in the present scenario, this phenomenon does not appear to be decisive, since many rational surfaces find close proximity to the peak of ω_* even at low toroidal mode numbers. Stated differently, the critical toroidal mode number for which rational surface alignment is important (see Ref. 62 for details) is very low for this discharge. The critical mode number is

$$n_{crit} = \frac{\rho_{tor}}{2\hat{s}q\mu_{crit}}, \tag{1}$$

where n_{crit} is the critical toroidal mode number, ρ_{tor} is the normalized radial flux surface coordinate, q is the safety factor $d\phi/d\psi$, $\hat{s}$ is the magnetic shear $(1/q)(dq/dr)$, and μ_{crit} is the distance in ρ between the nearest rational surface and peak in ω_{*e}. For toroidal mode numbers that exceed n_{crit}, multiple rational surfaces are found within the range of $\delta\rho = 2\mu_{crit}$, and the modes are not subject to an offset stabilization effect.[59] The value of n_{crit} for this discharge is ≈4. Therefore, at toroidal mode numbers above $n = 4$, instabilities are not suppressed by misalignment between the rational surfaces and the ω_* profiles.

Growth rates and frequencies are shown in Fig. 5 for both local and global linear simulations. As can be seen, there are multiple branches (peaks). We first demonstrate that the modes are MTMs and subsequently probe the distinction between the branches.

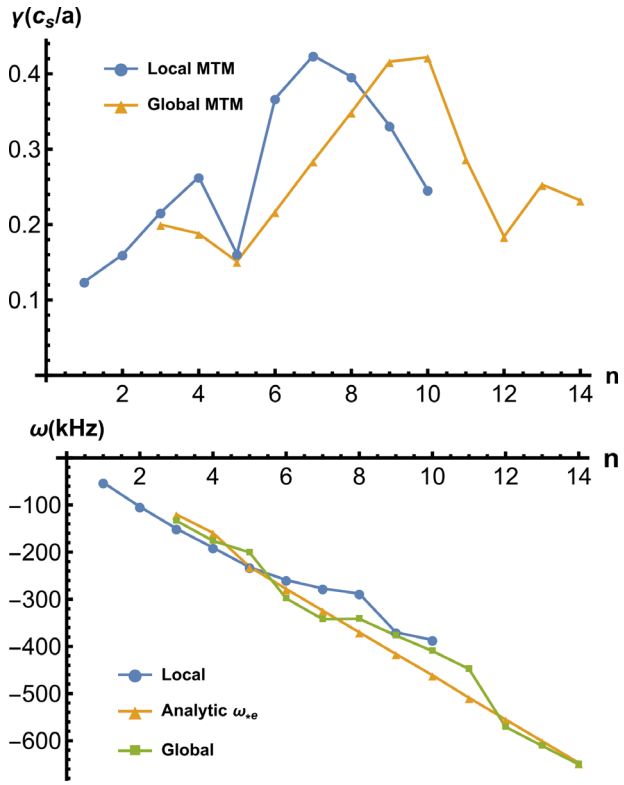

FIG. 5. Growth rates (top) are normalized to sound speed over characteristic length scale (c_s/a) as a function of binormal wavenumber $(k_y\rho_i)$ for local (blue) and global (gold) simulations. Local simulations are performed at the $\rho = 0.96$ radial flux surface, with profile input taken directly from experimental equilibrium reconstructions. Real frequencies (bottom) for local (blue) and global (green) simulations and the maximum value of the ω_{*e} profile (gold) in kHz.

To establish these modes as MTM, we first note that the experimental frequencies (≈100–400 kHz) closely match the MTM expectation for the given profiles: $\omega = \omega_{*e} = k_y\rho_s c_s\left(\frac{1}{L_{Te}} + \frac{1}{L_n}\right)$, which results in frequencies in the range of $\omega_{*e} = 120$–500 kHz for toroidal mode numbers $n = 3$–14 (we will describe detailed comparisons between GENE simulations and the spectrogram below).

GENE calculates heat flux using $Q = \int d^3v \frac{1}{2} mv^2 f_1 \mathbf{v}_D$, where $\mathbf{v}_E$ is the generalized $\mathbf{E} \times \mathbf{B}$ velocity, which can be separated into electrostatic $(v_{E,ES} \propto \delta\phi)$ and electromagnetic $(v_{E,EM} \propto \delta v_\parallel A_\parallel)$ components. Figure 6 depicts the ratio Q_{EM}/Q_{ES} for the global linear simulations, for which a high value is a hallmark of the MTM. An additional point in favor of the MTM is the tearing parity of the $A_\parallel$ eigenfunction shown in Fig. 7. Both the real and imaginary parts are roughly symmetric about $z = 0$, indicating even parity for the parallel component of the magnetic vector potential.

Finally, the transport ratios shown in Fig. 8 indicate that the electron channel dominates the observed heat flux $(\chi_i/\chi_e \ll 1)$, and the particle flux for each species is small in comparison with the electron heat diffusivity $(D_s/\chi_e \ll 1)$. Although this is also a signature of ETG modes, they can be excluded on the basis of the strong electromagnetic

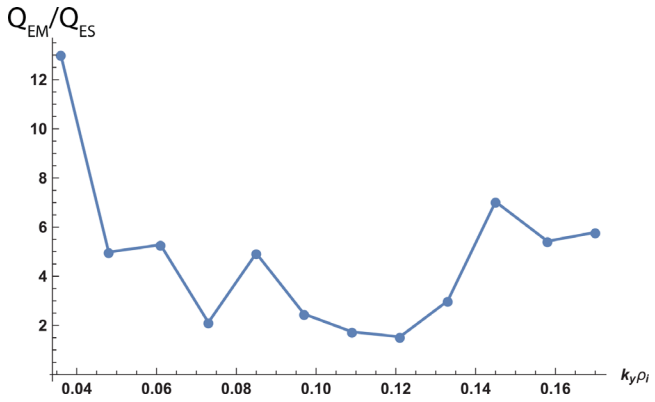

FIG. 6. Plot of the ratio of electromagnetic to electrostatic electron heat flux for a series of global GENE simulations of shot 174082. For MTMs, this ratio is expected to be > 1.

component of the flux and the large scales at which these modes are unstable.

B. Two MTM branches

Reference 31 demonstrates that two branches of MTM coexist in the DIII-D pedestal: a slab-like MTM at low n and a toroidal mode at higher n. These branches have distinct physical characteristics: the slab branch is insensitive to changes in ballooning angle and cannot exist in collisionless plasmas. By contrast, the toroidal mode is dependent on both collisionality and ballooning angle and can exist in collisionless systems. The coexistence of these two branches may offer insight into the virulence of microtearing modes across discharges.

As we show here, we identify the same phenomenon in this discharge, suggesting that it may be quite common in the pedestal. In contrast with Ref. 31, the toroidal branch in this discharge is unstable at lower toroidal mode numbers and in closer proximity (in n) to the slab branch.

We first examine the ballooning-angle dependence of two modes representative of the two branches, which is shown in Fig. 9 (this can only be examined for local linear simulations). The low-n mode exhibits very weak θ_0 dependence in contrast with the strong dependence of the high-n mode consistent with the characterization of each as slab or toroidal, respectively. The lower frequency electromagnetic fluctuation is associated with a lower toroidal mode number, due to the linear dependence of ω_{*e} on $k_y\rho_i$. Sharp changes in the frequency of the $n = 10$ simulations are likely due to transitions between similar MTM mode branches.

We also investigate the collisionality dependence of the modes. As shown in Fig. 10, the high-n branch asymptotes to a constant, non-negligible, growth rate corresponding to a mode that retains MTM characteristics in the low collisionality limit. In contrast, the low-n branch transitions to an ion diamagnetic-directed instability with very low growth rate as collisionality approaches zero, indicating that this low-n MTM is strongly stabilized and becomes subdominant to another mode in this limit. Once again, this collisionality dependence is consistent with the modes' characterization as slab like and

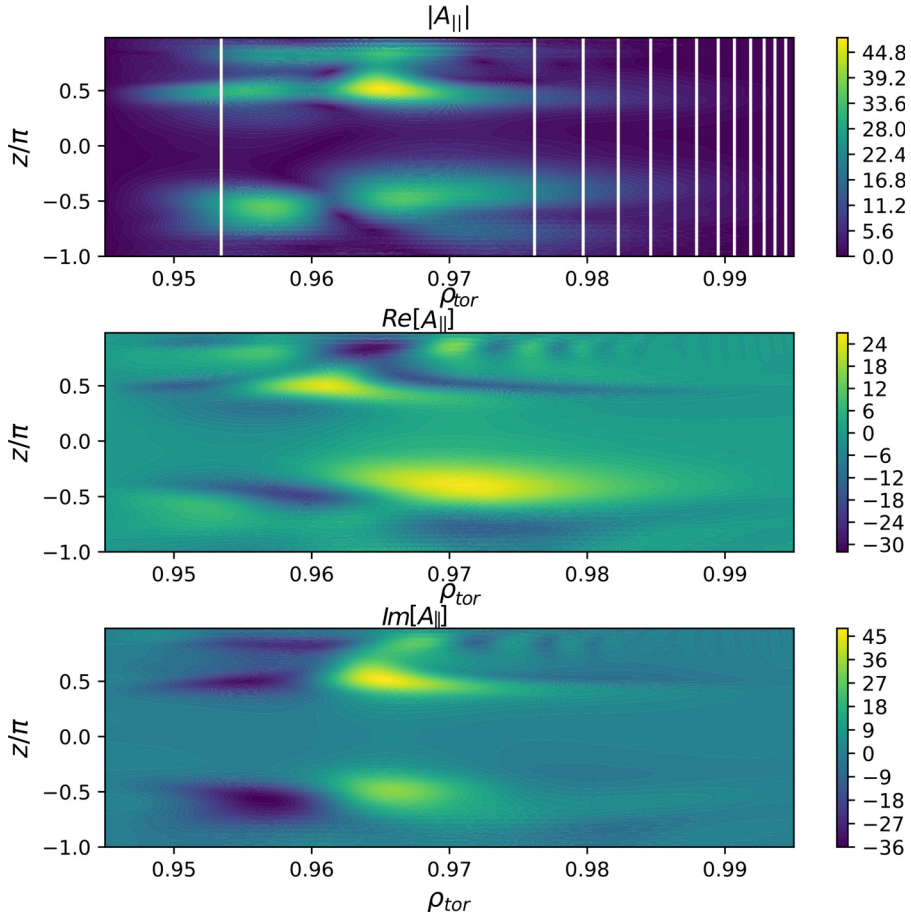

FIG. 7. Example contour of parallel component of the magnetic vector potential for a global linear GENE simulation ($n = 10$). Amplitudes are arbitrary as the simulation is linear. The mode structure displays tearing parity as $A_{||}$ is (predominantly) an even function.

curvature driven. Several recent papers have investigated (analytically and numerically) collisionless microtearing instabilities.[31,60,61]

C. Neoclassical transport

While the anomalous transport in the edge region is of considerable interest, a significant portion of ion heat flux can be attributed to neoclassical transport. Using the code NEO,[63,64] the neoclassical transport levels for ions, electrons, and impurities are calculated. Figure 11 shows the total neoclassical heat loss from all three species, primarily in the main ion channel, indicating that neoclassical transport is significant, particularly toward the pedestal top. Pedestal top ($\rho \approx 0.94$) neoclassical heat losses are significant and decrease in the steep gradient region. For reference, we expect a total of 4.67MW of power losses in the pedestal, so these transport levels are significant. Figure 12 shows the total particle loss due to neoclassical transport. Although neoclassical transport is generally weak in the particle channel, these particle transport levels are close to those predicted by SOLPS modeling:[30] $\sim 10^{21}$ particles/s. The code SOLPS predicts D and χ by iterating their value until modeled profiles ($n_e, T_e, n_i, T_i, P_{tot}$) match experimental predictions.[11] In summary, these results suggest that neoclassical transport is important in the ion heat channel and in the particle channel.

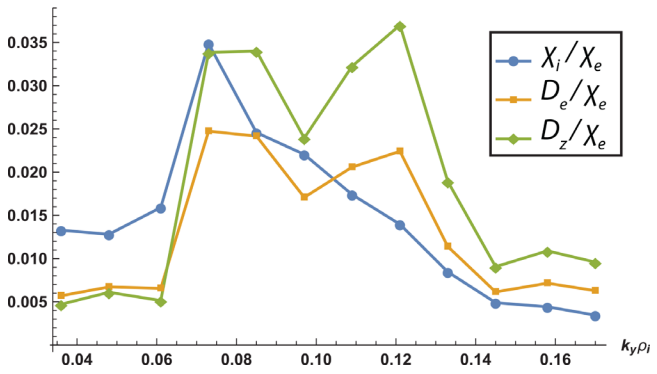

FIG. 8. Transport ratios of global linear simulations of the 174082 pedestal. These ratios are expected to be very small for both ETG and MTM instabilities.[2]

D. Local nonlinear simulations

To obtain estimates of anomalous power losses, fluctuation amplitudes, and transport coefficients, nonlinear simulations are required. Simulations of local nonlinear ETGs are performed at multiple radial locations in the pedestal by setting $k_{y,min}\rho_i = 5$ and $k_{y,max} = 240$, with sensitivity tests in the gradient drive to ensure that

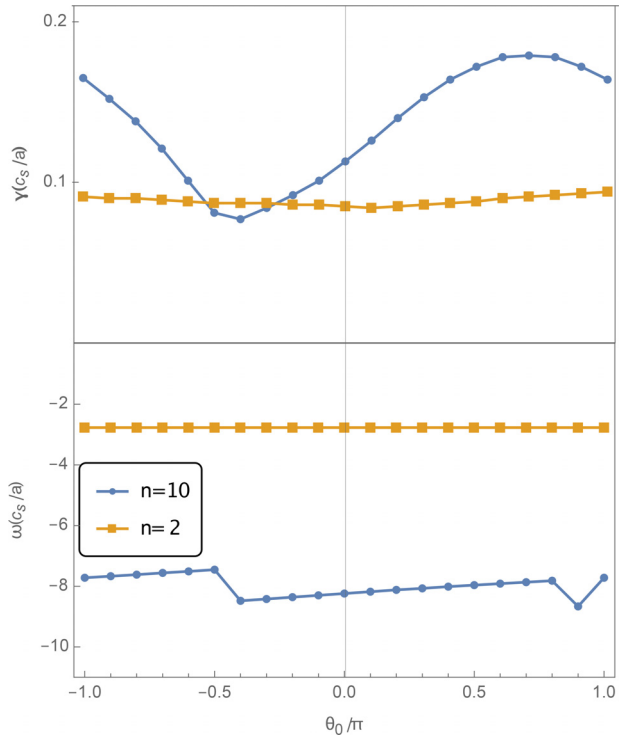

FIG. 9. Scan of ballooning angle for the $n = 2$ and $n = 10$ local linear instabilities. The change in growth rates with respect to ballooning angle for high-n modes is expected (due to toroidal effects), while the low-n modes are insensitive to ballooning angle (due to their slab-like nature).

variations in the equilibrium profiles do not result in major changes to transport coefficients at that location, increasing $\nabla T_e/T_e$ by 20% and decreasing $\nabla n_e/n_e$ by 20% to keep ∇P_e fixed. Simulations of neoclassical heat losses are performed at the same radial locations as the ETG,

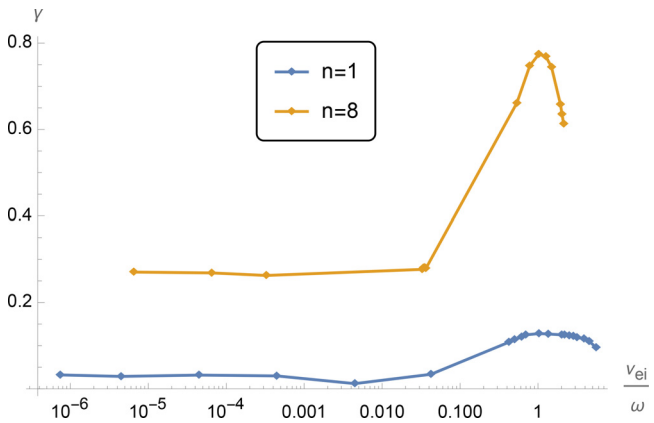

FIG. 10. Dependence of local microtearing growth rates as a function of electron–ion collisionality. For this scan: $\rho_{tor} = 0.96$, $k_y\rho_i = 0.15$ for the $n = 8$ simulation and $k_y\rho_i = 0.02$ for the $n = 1$ simulation. Non-monotonic dependence on collisionality is a key characteristic of MTMs[62] and is shown quite clearly for both $k_y\rho_i$ s. Note the persistence of MTM instability in the collisionless limit for the $n = 8$ mode.

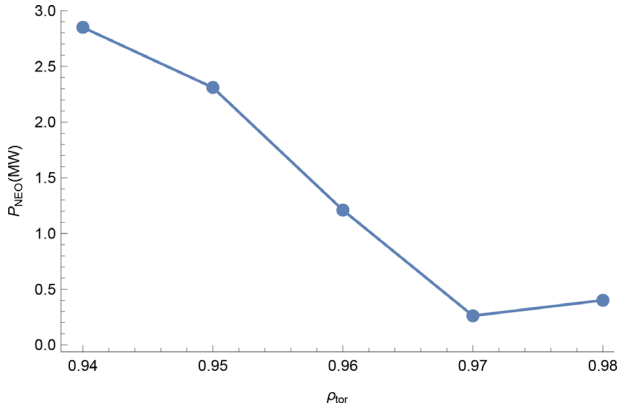

FIG. 11. Neoclassical heat transport across the pedestal as calculated with NEO. Pedestal top losses are significant but drop by mid-pedestal.

with their value indicated by the blue-shaded region. The nominal profiles resulted in insignificant electron heat flux ($P_{ETG} = 0.015$ MW at its highest), and the modified profiles gave much higher losses ($P_{ETG} = 1.26$ MW at its highest), but the resulting increase in energy loss is still not enough to account for the experimentally observed losses as shown by the purple region in Fig. 13.

Nonlinear simulations ($k_{y,min}\rho_i = 0.02$–0.24) of microtearing modes were carried out at the location of highest ∇T_e. The simulations extend from $k_y\rho_i = 0.02$–0.94 and employ kinetic electrons and adiabatic ions. The result is a high level of magnetic flutter ($Q_{em} = 1.14$ MW). An additional simulation with the same increase in $\nabla T_e/T_e$ by 20% and decrease in $\nabla n_e/n_e$ by 20% results in $Q_em = 1.32$MW. Even with the modified gradients, there is still some heat flux deficit (1.5 out of 4.7 MW), particularly at the outermost point. This may be an indication of some deficiency in modeling tools, neglect of additional relevant transport mechanisms, and/or a consequence of the intrinsically uncertain input data. Clearly, however, the transport mechanisms considered are at experimentally relevant levels.

The snapshot of magnetic vector potential depicted in Fig. 14 shows a contour plot of the fluctuations caused by the microtearing modes. The corresponding heat flux spectrum is shown in Fig. 15.

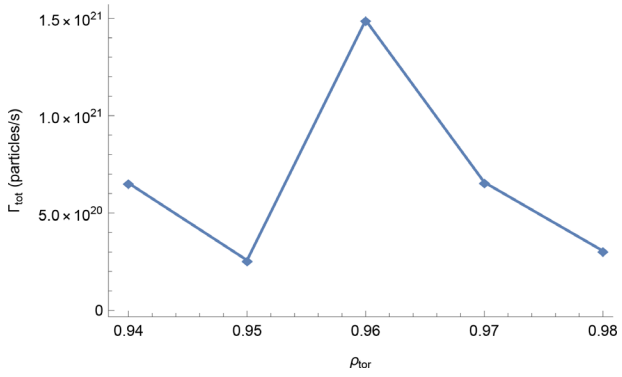

FIG. 12. Neoclassical particle fluxes across the pedestal calculated with NEO. Values are consistent with the results of SOLPS calculations of particle flux.

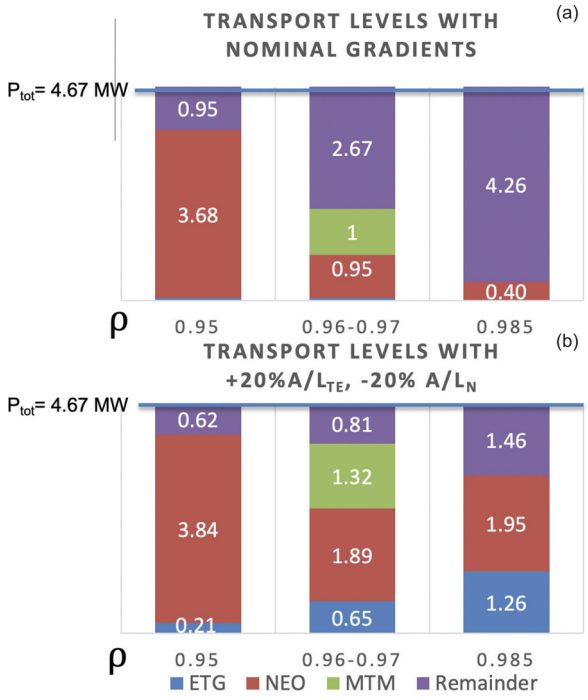

FIG. 13. Power losses at different radial locations across the pedestal, with no modification to the profile data (a). Power losses across the pedestal with modified temperature and density gradients (b).

Sensitivity studies of nonlinear microtearing saturation are under way, with variation of multiple driving mechanisms including β, ∇T_e, and ν_{ei} with the target of formulating reduced models for pedestal MTM transport. The effect of E × B shear was tested and found to be negligible for this parameter point.

E. Microtearing diffusivity model

In this section, we compare predicted electromagnetic transport levels with a simple model relating heat diffusivity as directly proportional to the fluctuation amplitude through a Rechester–Rosenbluth-like relation:[65]

$$\chi_e^{em} = \chi_{e\|}\langle(\tilde{B}_x/B_{ref})^2\rangle, \tag{2}$$

where the parallel diffusivity is given by

$$\chi_{e\|} \approx \frac{1}{k_\|}\left(\frac{T_e}{m_e}\right)^{1/2}. \tag{3}$$

The motivation is to characterize the extent to which the transport can be connected to the magnetic fluctuation level. This will inform, for example, interpretation of interior magnetic fluctuation diagnostics.[28]

To test the validity of this model, we compare this estimate with the results found in GENE. In the nonlinear GENE simulation of this discharge, the electromagnetic electron heat diffusivity is found to be $\chi_e^{em} = 0.16\mathrm{m}^2/\mathrm{s}$ and the $\tilde{B}_x/B_0 = 0.055$; this magnetic fluctuation amplitude is then used in a series of analytic predictions for electromagnetic heat flux. The calculation using the $k_\|$, calculated as an eigenfunction average of the parallel derivative at the peak linear growth rate (justified by the common observation that linear modes persist in the nonlinear turbulence) and the magnetic fluctuation amplitude from the nonlinear simulation, gives $\chi_e^{em} = 0.68\mathrm{m}^2/\mathrm{s}$, which is reasonably close to the nonlinear simulation (i.e., same order of magnitude, ∼4 times larger).

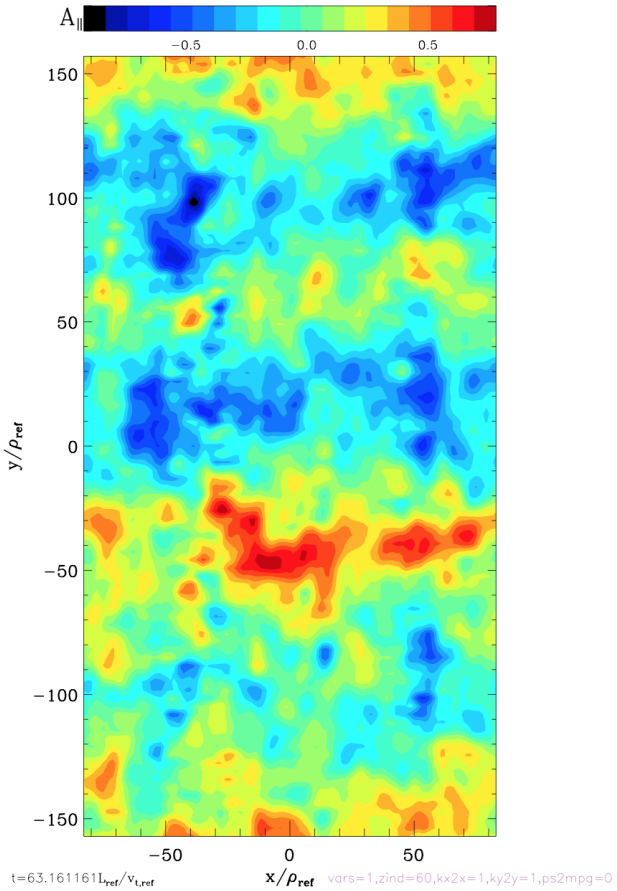

FIG. 14. Snapshot of $A_\|$ from a local nonlinear microtearing simulation. The dependence of the saturation amplitude on ballooning angle is observed. Strong electromagnetic heat flux is found at an experimentally relevant level, $Q_{em} = 1.14$ MW. Electrostatic heat flux is far below the electromagnetic component, $Q_{es} = 0.05$ MW.

The use of the Rechester–Rosenbluth formula to model χ_e^{em} by using the k_z extracted from the nonlinear structure and $\tilde{B}_x/B_0$ from the nonlinear simulation fares quite well, $\chi_e^{em} = 0.355$ (a factor of ∼2 discrepancy). Estimating the diffusivity using the standard approximation $1/k_\| = q_0 R$ fares much more poorly: $\chi_e^{em} = 2.61\mathrm{m}^2/\mathrm{s}$. Figure 16 compares these diffusivities and the method of $k_\|$ or $\chi_{e,\|}$ used in their calculation.

Ultimately, this exercise shows that heat flux from magnetic flutter may be estimated (to within an order of magnitude) from experimental data, provided accurate observations of magnetic fluctuation amplitudes and parallel wavenumbers.

F. Global and local scans of MHD-like modes

Motivated by the low-frequency activity in the magnetic spectrogram, we investigate low-frequency MHD instabilities by studying

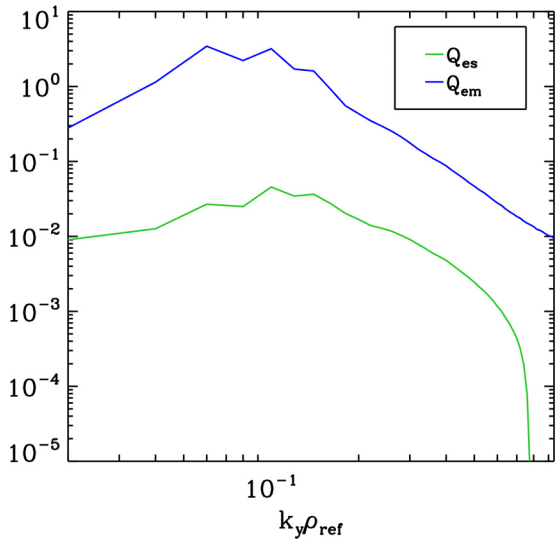

FIG. 15. Flux spectrum for a local nonlinear microtearing mode, in GyroBohm units $c_s n_0 T_0 \rho_*^2$, where c_s is the sound speed $\sqrt{(T_{e0}/m_i)}$, n_{e0} is the electron density, T_{e0} is the equilibrium electron temperature, and ρ_* is the ratio of gyroradius to machine length scale ρ/a. The electromagnetic component, Q_{em} (blue), is significantly higher than the electrostatic flux, Q_{es} (green).

modified scenarios that produce such modes. Unstable local MHD modes are quite easy to produce. However, global MHD modes are much more challenging to produce for this scenario.

These results are obtained by increasing the pedestal β to levels surpassing the nominal experimental value ($\beta = 0.003\,125$ at the center of global MTM simulations) without modifying the equilibrium profiles. By increasing the value of the pedestal beta by a factor of 2.4 for global ($\beta = 0.0075$) and 1.8 ($\beta_{nom} = 0.001$ and $\beta_{mod} = 0.001\,88$) for flux-tube simulations, keeping the profile gradients fixed, we

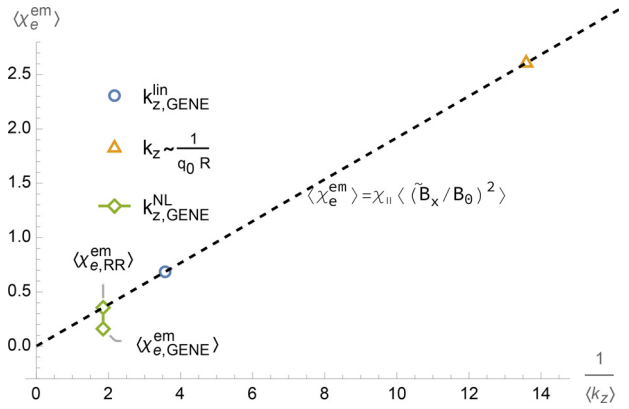

FIG. 16. Plot of electromagnetic electron heat diffusivity as modeled by the Rochester–Rosenbluth model defined in Eq. (2). The bottom green diamond represents the diffusivity calculated directly from nonlinear GENE simulations. The remaining symbols denote the model prediction using various estimates of the parallel wavenumber. There is reasonable agreement between the model and the nonlinear simulation using the parallel wavenumber calculated directly from the nonlinear simulation (top green symbol).

identify unstable MHD modes. These values of β are clearly beyond experimental uncertainties. However, two considerations suggest that MHD modes may be unstable at more realistic values of β: (1) the mode is likely unstable at much lower values of β, but it is subdominant to MTM, and (2) for global simulations, the mode is likely more unstable with a more realistic radial boundary condition. The radial boundary condition for GENE simulations is a Dirichlet boundary conditions just inside the separatrix (MHD stability is well known to depend sensitively on the vacuum region). Moreover, there are additional uncertainties in density and temperature gradients as well as magnetic geometry (notably magnetic shear) that could be probed.

For the lowest toroidal mode numbers with unrealistically large β values, the resulting MHD-like instability becomes the most unstable mode. The real frequencies and growth rates for both local and global MHD-like simulations are shown in Fig. 17. Figure 18 shows transport ratios for a set of high-β simulations, which are consistent with the expectations from Ref. 2 for MHD-like modes. Note that the global simulations include the Doppler shift from flow shear, but the local simulations do not, which should be considered in the context of the mode frequencies shown in Fig. 17.

The characteristics of these modes are consistent with expectations of MHD-like modes, namely, significant particle diffusivity relative to heat diffusivity, real frequencies in the ion diamagnetic direction, similar heat transport in the ion and electron channels

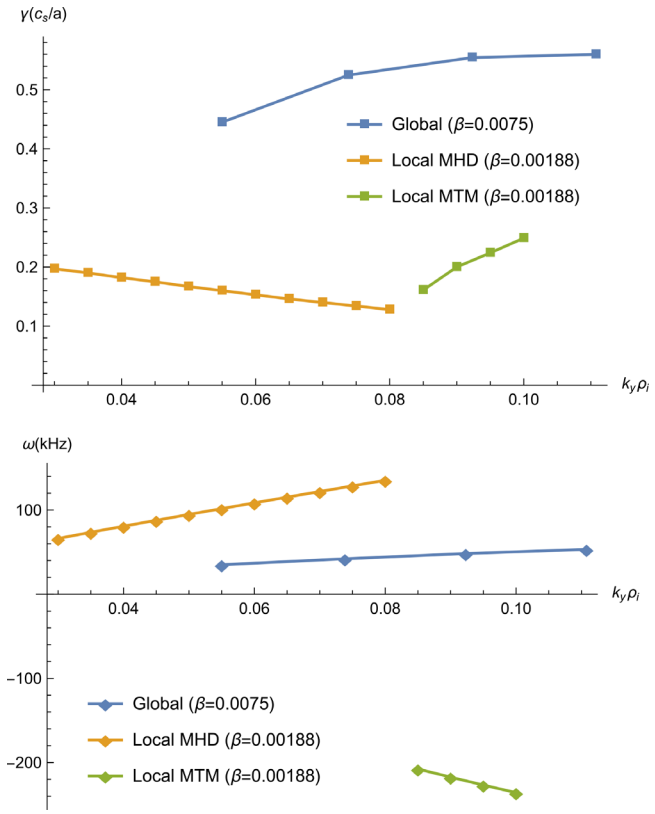

FIG. 17. Growth rates (top) and real frequencies (bottom) of global MHD modes (blue), local MHD instabilities (orange), and local microtearing instabilities (green) for modified β simulations.

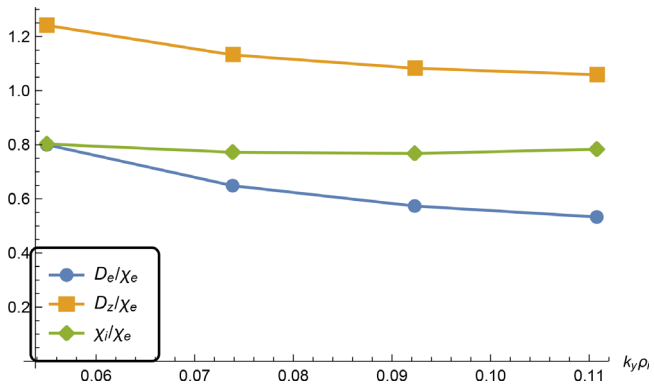

FIG. 18. Transport ratios for global simulations with $\beta = 0.0075$. Values are consistent with the "fingerprints" of MHD-like modes.

($\chi_i/\chi_e \approx 1$), and heat transport dominated by electrostatic fluctuations ($Q_{em}/Q_{es} < 1$). The global instability appears to be an Alfvénic mode, as it satisfies the relation $\omega \approx k_\parallel v_A$ rather than the KBM dispersion expectation of $\omega \approx \omega_i^*/2$. The parity appears to be ballooning, rather than tearing, as shown in Fig. 19. Further investigation into the nature of this instability is left for future work.

Another "fingerprint" that distinguishes microtearing instabilities from MHD-like modes comes in the form of parallel electric field cancelation. In kinetic MHD modes, $E_\parallel$ is near zero while microtearing modes have a finite electric field linked to Ohm's law and the current that is driven around the rational surfaces. Figure 20 shows the normalized electric field cancelation factor as calculated by

$$\hat{E}_\parallel = \frac{\int dz|-\partial_z\phi + i\omega A_\parallel|}{\int dz|\partial_z\phi| + \int dz|i\omega A_\parallel|}, \tag{4}$$

differs significantly between MTM and MHD instabilities.

We note that this $E_\parallel$ criterion for MHD modes is more robust the closer the mode is to ideal MHD, i.e., $E_\parallel \approx 0$ for ideal MHD modes, while a residual $E_\parallel$ exists for their kinetic analogue. Extended MHD codes such as NIMROD[66] have the capacity to model considerable non-ideal behavior. Consequently, such MHD codes are clearly not constrained to model $E_\parallel \sim 0$ modes and the MHD-like transport ratios that stem from this constraint.[2] For highly electrostatic modes, i.e., ETGs, this ratio nears unity. MTMs are found to have significant $A_\parallel$ and ϕ, leading to $E_\parallel \approx 0.5$.

IV. COMPARISON OF TRANSPORT AND FLUCTUATIONS FROM MTM AND MHD

In this section, we will compare MTMs with MHD modes with the goal of drawing conclusions about their respective roles in pedestal transport. To that end, we will examine the sets of gyrokinetic

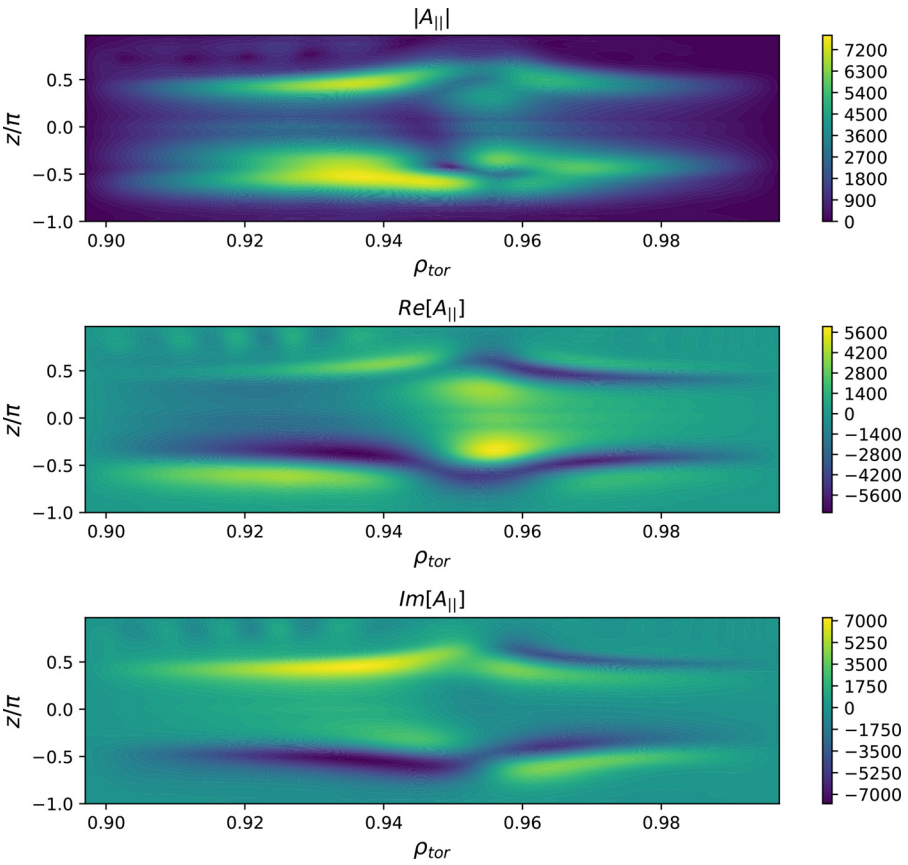

FIG. 19. Contour plot of $A_\parallel$ for the MHD-like instability. The mode has odd (ballooning) parity and is radially extended.

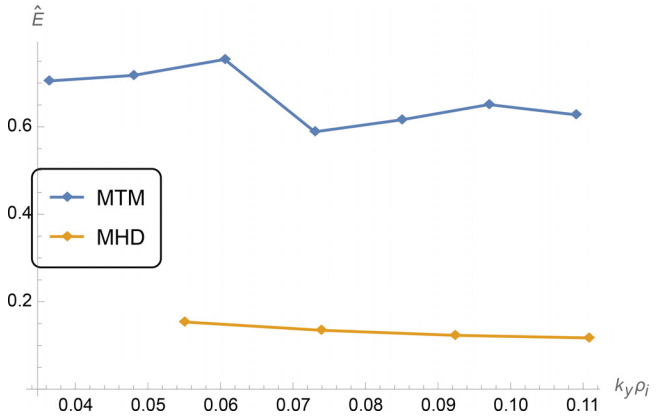

FIG. 20. Measure of $\hat{E}_{||}$ for simulations with baseline (blue) and modified (gold) profiles. The MHD-like instabilities resulting from increased β have significant parallel electric field cancelation, while the nominal microtearing cases have a finite parallel electric field.[2]

simulations described above: (1) global and local linear MTMs, (2) local nonlinear MTMs, and (3) global and local linear MHD modes with modified β. Each set of simulations has its inherent strengths and weaknesses. The global linear MTM simulations capture background profile variation, which has been shown to be important in the past, and include kinetic ions (allowing for particle flux information) but do not predict fluctuation levels. The local nonlinear MTM simulations neglect background profile variation and kinetic ions but do predict a nonlinear saturation amplitude and heat flux. Nonlinear MHD simulations using gyrokinetics are extremely challenging, and so we limit the investigation to linear. The global linear MHD simulations with $2.4\beta_{nom_global}$ include background profile variation and information regarding the width of the drive region,[67] but extremely high β is required to produce an MHD mode.[68,69] In contrast, the local linear MHD simulations with $1.8\beta_{nom,local}$ neglect the radially nonlocal effects but do not require such extreme values of β to destabilize as their global counterpart.

These simulations will be examined in the context of the following experimental (or edge modeling) data:

- Magnetic spectrograms.
- The ratio of density fluctuation amplitude to heat flux.
- The ratio of magnetic fluctuation amplitude to density fluctuation amplitude.
- The ratio of particle flux to heat flux (calculated from SOLPS simulations).

For some of these analyses, it is important to keep in mind that experimental diagnostics often target the outboard midplane. For instabilities such as the ITG (in the core) or KBM, this coincides with the peak fluctuation amplitude. However, microtearing instabilities in the pedestal peak off-axis, leading to a minimum in fluctuations at the outboard midplane. Figure 21 depicts the ratio of line-averaged magnetic to density fluctuations as a function of height (above or below the outboard midplane). Consequently, although measures of outboard midplane fluctuations are highly useful, they are not able to diagnose important aspects of our MTM predictions.

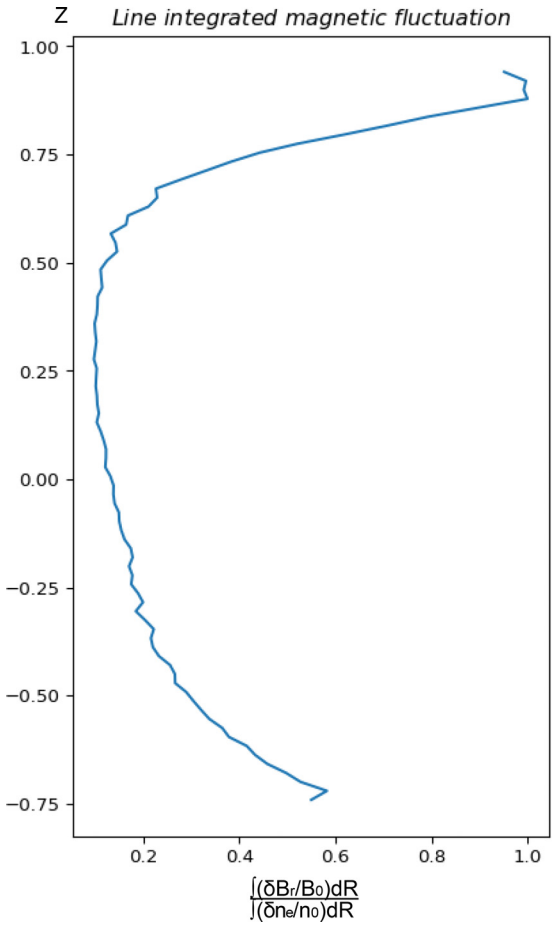

FIG. 21. Ratio of normalized line-integrated magnetic fluctuation to normalized density fluctuation calculated using a representative GENE MTM simulation.

A. Magnetic spectrograms

Figure 22 shows that the fastest-growing linear MTM is approximately at the same real frequency (∼400 kHz) as the experimentally observed signal in Fig. 1. The lower band in the spectrogram $f \sim 100$–200 kHz is also quite close to the frequency of the low k_y MTM peak (slightly over 100 kHz). The experimentally observed frequency range is the broadest at the time from which the equilibrium data were acquired ($t = 3000$ ms), which is perhaps consistent with the unstable MTMs in the simulations spanning the whole frequency range.

There is also a low-frequency band in the spectrogram (circled in black in Fig. 1), which we will compare with the MHD frequencies. The mode frequencies of the (global, which accounts for the Doppler shift) simulated MHD instabilities range from 35 to 55 kHz (recall Fig. 17), consistent with this band.

In summary, the higher frequency bands correspond quite well with the peaks in the global MTM growth rate spectrum, while the lower band corresponds quite well with the simulated MHD modes. We find it plausible that both are active simultaneously in the pedestal and affect different transport channels. The MTM instabilities would

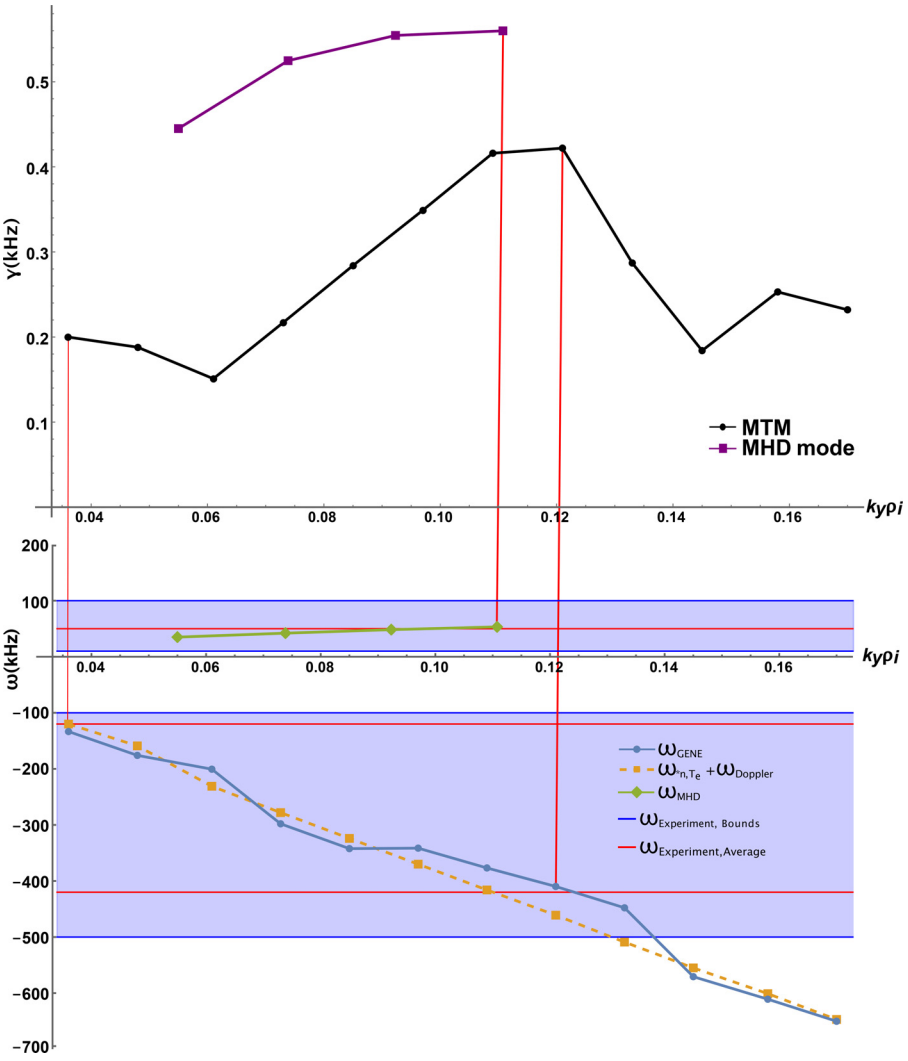

FIG. 22. Plot of growth rates (top) and real frequencies (bottom) for a spectrum of microtearing and MHD modes in shot 174082. The real frequencies obtained from GENE (blue circles) are compared with the electron diamagnetic frequency (yellow squares) and the experimentally observed magnetic fluctuation ranges (blue-shaded regions).

mediate the electron heat flux and temperature profiles, while the MHD modes would be limited primarily to particle transport.[2] We further explore the plausibility of this picture in Secs. IV B–IV D.

B. Ratio of magnetic fluctuation amplitude to density fluctuation amplitude

The ratio of magnetic fluctuations to density fluctuations is also a quantity that could differ between modes and can be measured by the recently developed Faraday effect radial interferometer–polarimeter (RIP) diagnostic[28,29] (although such fluctuation measurements are not available for this discharge).

MHD-like modes are expected to exhibit higher $\frac{\overline{\delta n}/n}{\overline{\delta B}/B}$ in comparison with MTM modes at the outboard midplane. However, simulations of the increased β equilibria show that the MHD-like modes exhibit a $\frac{\overline{\delta B}/B}{\overline{\delta n}/n}$ ratio that is similar to (and, in fact, generally larger than) their microtearing counterpart, as shown in Fig. 23. Experimental expectations for KBMs predict that this ratio would be an order of magnitude

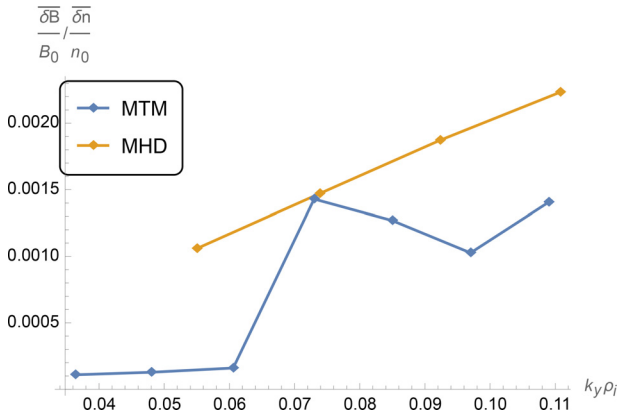

FIG. 23. The ratio of $\frac{\delta B/B}{\delta n/n}$ is calculated for simulations of both the baseline equilibrium profiles and profiles with modified β_e with the integration taking place across the midplane.

lower than the value from MTMs. These MHD modes producing a higher value than their MTM counterpart is further evidence that this instability is unlikely to be a KBM. Consequently, this metric alone cannot cleanly discriminate between MTMs and all MHD-like modes, and thus, the following other quantities must also be compared.

C. Ratio of density fluctuation amplitude to heat flux

Here, we examine another prospective experimentally accessible metric, the ratio of density fluctuations to heat flux $(\delta n/n_0)/Q$. In this discharge, beam emission spectroscopy (BES) is used to place an upper bound on the possible density fluctuation level. Shot 174082 is distinctive because the density fluctuation amplitude falls below the noise level of BES measurements. This places an upper bound on the possible fluctuation levels ($\delta n/n \approx 0.1\%$), which we will use in comparison with simulated fluctuation amplitudes.

Figure 24 shows this ratio for the series of global MTM (blue solid line) and MHD (gold solid line) simulations, as well as for the threshold experimental fluctuation level $\delta n/n \approx 0.1\%$ described above (gray solid line) and the local nonlinear microtearing simulation (gold dashed line). As shown in Fig. 24, the nonlinear MTM simulation produces a ratio quite close to this experimental estimate. However, the estimate from linear MHD is somewhat larger. Since this density fluctuation level is an upper bound, this would imply that the MHD mode is unlikely to account for the bulk of the heat flux. This does not eliminate the possibility of MHD fluctuations since (1) the value of $(\delta n/n_0)/Q$ for the MHD modes is not too much larger than the experimental upper bound, and (2) even at a low fluctuation level, the MHD modes could still strongly impact the particle transport channel.

No conclusions can be drawn from the diagnostic signals regarding the significance of the density fluctuations. However, this information can be used to constrain our numerical experiments. The diagnostics show that the density fluctuations cannot exceed a certain value. That information gives insight from the set of linear simulations. The linear simulations do not provide transport levels (i.e., fluxes) or fluctuation levels, but they do provide ratios between these quantities.

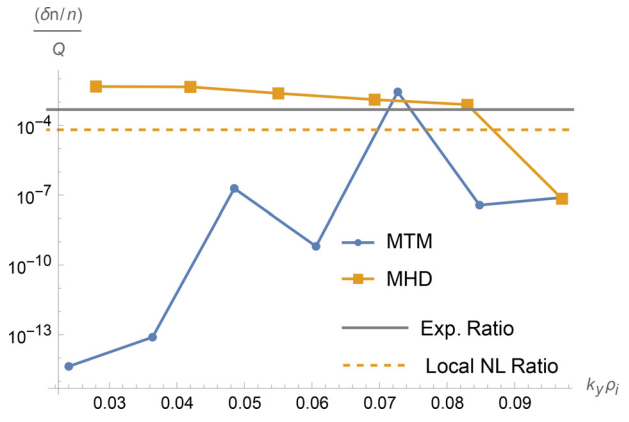

FIG. 24. Ratio of $(\delta n/n_0)/Q$ for both microtearing and MHD-like global simulations. The gray solid line is calculated using the experimental noise floor of the BES diagnostic ($\delta n/n_0 = 0.001$) and an estimate of anomalous power lost in this discharge ($Q = 2.1$MW). The yellow dashed line is the ratio from a local nonlinear simulation of shot 174082 ($\delta n/n_0 = 0.000\,073\,247\,8$, $Q = 1.14$ MW).

The lack of a density fluctuation signal places an upper bound on the density fluctuations for a given mode, which then, in turn, constrains the possible contribution of that mode to the various transport channels. In summary, this analysis is consistent with the nonlinear MTM simulations described above but cannot rule out the possibility of MHD fluctuations as well. The combined MTM and MHD scenario proposed above remains a possibility.

D. Ratio of particle flux to heat flux

As a final comparison between MHD and MTM, we compare the ratio of particle to heat flux. A robust feature of MHD modes is that they produce roughly equal diffusivity in the particle and heat channels: $D \sim \chi$ (this criterion is increasingly stringent with proximity to the ideal MHD limit). In contrast, MTMs produce much higher heat transport: $D/\chi \ll 1$. The particle diffusivity is difficult to diagnose experimentally, but edge modeling can provide an estimate. SOLPS was used to this end for this discharge as described in Ref. 30.

Figure 25 depicts the values of Γ_{tot}/Q_{tot} for the linear simulations of MTMs (global) and MHD-like modes (global and local) along with the SOLPS[11] iterative model (recall that these nonlinear MTM simulations cannot be used here because of the adiabatic ion approximation). The unstable microtearing modes agree with the value found in SOLPS, whereas the MHD modes exceed the SOLPS prediction. Local values of Γ_{tot}/Q_{tot} in kinetic MHD modes are comparable with their global counterparts. If the MHD modes are active, their impact would be largely limited to the particle channel as shown by the significant particle to heat flux ratios in both local and global simulations. Our conclusion from this analysis is similar to that of Sec. IV C: MHD modes may be active but only at a level that can impact the particle transport rather than the heat transport.

V. SUMMARY OF RESULTS

Global GENE simulations of DIII-D shot 174082 have shown that the most unstable mode for a series of toroidal wavenumbers, with real frequencies corresponding to a broad band of observed magnetic fluctuations, is a microtearing mode. Simulations also indicate that ETG turbulence and neoclassical effects cannot account for the total heat transport observed in this shot. A significant cause of energy

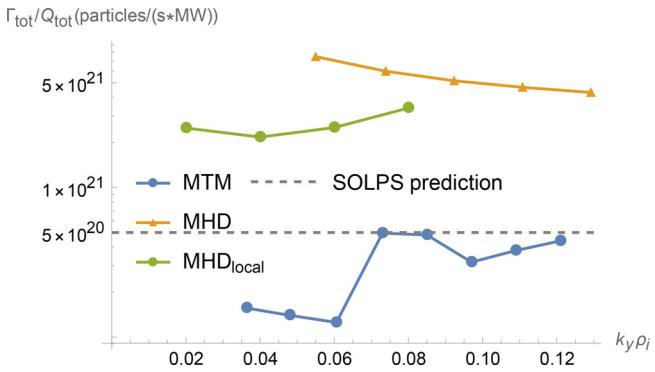

FIG. 25. Ratio of total surface-averaged particle flux, Γ, to total heat flux, Q, in SI units for each respective quantity. The ratio of particle fluxes to heat fluxes is predicted to be higher for MHD-like instabilities than MTMs.[2] This is confirmed for global GENE simulations of these instabilities.

loss in the pedestal is found to be the microtearing mode, as evidenced by a combination of nonlinear local, linear local, and linear global simulations of the pedestal region. The MTM is the fastest-growing linear instability, with gyrokinetic fingerprints that correspond well with the expectations of analytic theory, the observations of experimental diagnostics, and the resulting gyrokinetic simulations of carefully reconstructed equilibria. Notably, the MTM frequencies are in good agreement with bands in the magnetic spectrogram.

Modifying the equilibrium β to 2.4× the nominal experimental value shows that an unidentified MHD mode, possibly a toroidal Alfvén eigenmode or ballooning mode, becomes unstable, with fluctuation frequencies consistent with a band of fluctuations observed in the experimental magnetic spectrogram. This low-frequency mode may be responsible for inter-ELM particle transport. Further characterization of this instability is left for a future project.

VI. CONCLUSIONS

This paper has investigated transport and magnetic fluctuations in the pedestal using gyrokinetic (using the GENE code) simulations for DIII-D discharge 174082. The main findings are as follows: Simulated MTM frequencies are in good agreement with corresponding frequency bands in the magnetic spectrogram, and nonlinear MTMs produce experimentally relevant transport levels. We conclude that it is very likely that MTMs are responsible for the observed magnetic fluctuations and that it is likely that they also limit the electron temperature pedestal. We also speculate that MHD modes are responsible for low-frequency fluctuations found in the magnetic spectrogram. Although GENE does not identify unstable MHD modes as the most unstable mode for the nominal equilibrium reconstruction, high beta ($\beta = 2.4\beta_{nom}$) simulations produce MHD modes with frequencies in the right range. Although this β value is clearly beyond experimental levels, other factors may suggest that MHD modes may be unstable at more realistic values of β, notably limitations of the GENE radial boundary condition and the possibility of subdominant instability.

We investigate several metrics that may inform or constrain the possible roles of MHD and MTMs. Two metrics are, perhaps surprisingly, ineffective at discriminating between the two classes of fluctuations. The ratio of density fluctuation amplitudes to magnetic fluctuation amplitudes is comparable for MHD and MTM based on linear GENE simulations. Likewise, the ratio of density fluctuation amplitudes to heat flux is somewhat larger for MHD modes, but not so large as to preclude their activity in this discharge. One metric, however, clearly distinguishes between MHD and MTM: the ratio of particle to heat diffusivity is much smaller for MTMs in agreement with SOLPS predictions. While this does not preclude the possible activity of MHD modes, it does limit their role to the particle transport channel.

We also investigate neoclassical and ETG as prospective transport mechanisms. Neoclassical transport (as calculated with NEO) produces substantial ion heat flux and particle flux roughly in agreement with SOLPS interpretive modeling. ETG transport is negligible for the nominal gradients. For simulations with moderately higher η (within experimental uncertainties), ETG transport becomes relevant although still somewhat below experimental expectations.

Two possible transport pictures emerge, (1) one without MHD fluctuations and (2) one including MHD fluctuations. In scenario (1) (negligible MHD fluctuations), neoclassical transport accounts for the particle channel and ion heat channel, while ETG and MTM supply the electron heat transport. Simulated values for these (neoclassical, ETG, MTM) transport mechanisms are consistent with this picture. In scenario (2), MHD combines with neoclassical to account for the particle transport, and other channels are the same as in scenario (1). Although we are unable to probe this possibility with nonlinear MHD simulations, there is a low-frequency fluctuation band in the spectrogram that may signal such MHD activity.

ACKNOWLEDGMENTS

This work is supported by U.S. DOE under Grant Nos. DE-FC02-04ER54698, DE-FG02-97ER54415, DE-AC02-09CH11466, and DE-SC0022164. A portion of this study's data analysis was performed using the OMFIT integrated modeling framework.[40] This manuscript has been authored by UT-Battelle, LLC, under Contract No. DE-AC05-00OR22725 with the U.S. Department of Energy (DOE). The publisher acknowledges the U.S. Government License to provide public access under the DOE Public Access Plan (http://energy.gov/downloads/doe-public-access-plan). This report was prepared as an account of work sponsored by an agency of the U.S. government. Neither the U.S. government nor any agency thereof, nor any of their employees, makes any warranty, express or implied, or assumes any legal liability or responsibility for the accuracy, completeness, or usefulness of any information, apparatus, product, or process disclosed, or represents that its use would not infringe privately owned rights. Reference herein to any specific commercial product, process, or service by trade name, trademark, manufacturer, or otherwise does not necessarily constitute or imply its endorsement, recommendation, or favoring by the U.S. government or any agency thereof. The views and opinions of authors expressed herein do not necessarily state or reflect those of the U.S. government or any agency thereof.

AUTHOR DECLARATIONS

Conflict of Interest

The authors have no conflicts to disclose.

Author Contributions

Michael R. Halfmoon: Conceptualization (lead); Data curation (lead); Formal analysis (lead); Investigation (lead); Methodology (equal); Validation (equal); Visualization (lead); Writing – original draft (lead); Writing – review & editing (lead). **Ehab Hassan:** Data curation (equal); Resources (equal); Software (equal); Writing – review & editing (equal). **Emily Ann Belli:** Formal analysis (equal); Resources (equal); Software (equal). **Jeff Candy:** Formal analysis (equal); Resources (equal); Software (equal). **David R. Hatch:** Funding acquisition (equal); Investigation (equal); Project administration (equal); Supervision (equal); Writing – review & editing (equal). **Michael Kotschenreuther:** Conceptualization (equal); Formal analysis (equal); Funding acquisition (equal); Methodology (equal); Supervision (equal); Visualization (equal); Writing – review & editing (equal). **Swadesh Mitter Mahajan:** Conceptualization (equal); Formal analysis (equal); Funding acquisition (equal); Investigation (equal); Supervision (equal); Writing – review & editing (equal). **Andrew Oakleigh**

Nelson: Data curation (equal); Investigation (equal); Resources (equal); Software (equal). **Egemen Kolemen:** Investigation (supporting); Resources (supporting); Supervision (equal). **Max Tian Curie:** Formal analysis (equal); Investigation (supporting); Resources (supporting); Visualization (equal). **Ahmed Diallo:** Formal analysis (equal); Investigation (equal); Validation (supporting). **Richard Groebner:** Conceptualization (equal); Funding acquisition (equal); Project administration (equal); Supervision (equal); Writing – review & editing (equal).

DATA AVAILABILITY

The data that support the findings of this study are available from the corresponding author upon reasonable request.

REFERENCES

[1]F. Wagner, G. Fussmann, T. Grave, M. Keilhacker, M. Kornherr, K. Lackner, K. McCormick, E. R. Müller, A. Stäbler, G. Becker *et al.*, "Development of an edge transport barrier at the H-mode transition of ASDEX," Phys. Rev. Lett. **53**(15), 1453 (1984).

[2]M. Kotschenreuther, X. Liu, D. R. Hatch, S. Mahajan, L. Zheng, A. Diallo, R. Groebner, J. C. Hillesheim, C. F. Maggi, C. Giroud *et al.*, "Gyrokinetic analysis and simulation of pedestals, to identify the culprits for energy losses using fingerprints," Nucl. Fusion **59**(9), 096001 (2019).

[3]F. Jenko, W. Dorland, M. Kotschenreuther, and B. N. Rogers, "Electron temperature gradient driven turbulence," Phys. Plasmas **7**(5), 1904–1910 (2000).

[4]D. Told, F. Jenko, P. Xanthopoulos, L. D. Horton, and E. Wolfrum, "Gyrokinetic microinstabilities in ASDEX upgrade edge plasmas," Phys. Plasmas **15**(10), 102306 (2008).

[5]D. R. Hatch, M. T. Kotschenreuther, S. Mahajan, P. Valanju, F. Jenko, D. Told, T. Görler, and S. Saarelma, "Microtearing turbulence limiting the JET-ILW pedestal," Nucl. Fusion **56**(10), 104003 (2016).

[6]D. R. Hatch, M. T. Kotschenreuther, S. Mahajan, P. Valanju, and X. Liu, "A gyrokinetic perspective on the JET-ILW pedestal," Nucl. Fusion **57**(17), 036020 (2017).

[7]D. R. Hatch, M. Kotschenreuther, S. M. Mahajan, G. Merlo, A. R. Field, C. Giroud, J. C. Hillesheim, C. F. Maggi, C. Perez von Thun, C. M. Roach *et al.*, "Direct gyrokinetic comparison of pedestal transport in jet with carbon and ITER-like walls," Nucl. Fusion **59**(8), 086056 (2019).

[8]B. A. Carreras, L. Garcia, and P. H. Diamond, "Theory of resistive pressure-gradient-driven turbulence," Phys. Fluids **30**(5), 1388–1400 (1987).

[9]P. B. Snyder, T. H. Osborne, K. H. Burrell, R. J. Groebner, A. W. Leonard, R. Nazikian, D. M. Orlov, O. Schmitz, M. R. Wade, and H. R. Wilson, "The EPED pedestal model and edge localized mode-suppressed regimes: Studies of quiescent H-mode and development of a model for edge localized mode suppression via resonant magnetic perturbations," Phys. Plasmas **19**(5), 056115 (2012).

[10]D. Dickinson, C. M. Roach, S. Saarelma, R. Scannell, A. Kirk, and H. R. Wilson, "Kinetic instabilities that limit β in the edge of a tokamak plasma: A picture of an H-mode pedestal," Phys. Rev. Lett. **108**, 135002 (2012).

[11]J. M. Canik, A. R. Briesemeister, C. J. Lasnier, A. W. Leonard, J. D. Lore, A. G. McLean, and J. G. Watkins, "Modeling of detachment experiments at DIII-D," J. Nucl. Mater. **463**, 569–572 (2015).

[12]R. D. Hazeltine, D. Dobrott, and T. S. Wang, "Kinetic theory of tearing instability," Phys. Fluids **18**(12), 1778–1786 (1975).

[13]J. F. Drake, N. T. Gladd, C. S. Liu, and C. L. Chang, "Microtearing modes and anomalous transport in tokamaks," Phys. Rev. Lett. **44**(15), 994–997 (1980).

[14]N. T. Gladd, J. F. Drake, C. L. Chang, and C. S. Liu, "Electron temperature gradient driven microtearing mode," Phys. Fluids **23**(6), 1182–1192 (1980).

[15]T. Rafiq, J. Weiland, A. H. Kritz, L. Luo, and A. Y. Pankin, "Microtearing modes in tokamak discharges," Phys. Plasmas **23**(6), 062507 (2016).

[16]T. Rafiq, A. H. Kritz, J. Weiland, L. Luo, and E. Schuster, "Study of the parametric dependence of linear and nonlinear microtearing modes in conventional tokamak discharges," Phys. Plasmas **25**(1), 012504 (2017).

[17]X. Jian, C. Holland, J. Candy, E. Belli, V. Chan, A. M. Garofalo, and S. Ding, "Role of microtearing turbulence in DIII-D high bootstrap current fraction plasmas," Phys. Rev. Lett. **123**, 225002 (2019).

[18]S. R. Haskey, A. Ashourvan, S. Banerjee, K. Barada, E. A. Belli, A. Bortolon, J. Candy, J. Chen, C. Chrystal, B. A. Grierson *et al.*, "Ion thermal transport in the H-mode edge transport barrier on DIII-D," Phys. Plasmas **29**(1), 012506 (2022).

[19]A. Ashourvan, R. Nazikian, E. Belli, J. Candy, D. Eldon, B. A. Grierson, W. Guttenfelder, S. R. Haskey, C. Lasnier, G. R. McKee, and C. C. Petty, "Formation of a high pressure staircase pedestal with suppressed edge localized modes in the DIII-D tokamak," Phys. Rev. Lett. **123**, 115001–115Sep (2019).

[20]K. Stimmel, A. Bañón Navarro, T. Happel, D. Told, T. Görler, E. Wolfrum, J. P. Martin Collar, R. Fischer, P. A. Schneider, and F. Jenko, "Gyrokinetic investigation of the ASDEX upgrade I-mode pedestal," Phys. Plasmas **26**(12), 122504 (2019).

[21]J. Chowdury, Y. Chen, W. Wan, S. E. Parker, W. Guttenfelder, and J. M. Canik, "Particle-in-cell δf gyrokinetic simulations of the microtearing mode," Phys. Plasmas **23**(1), 012513 (2015).

[22]D. R. Hatch, M. T. Kotschenreuther, S. M. Mahajan, M. J. Pueschel, C. Michoski, G. Merlo, E. Hassan, A. R. Field, L. Frassinetti, C. Giroud *et al.*, "Microtearing modes as the source of magnetic fluctuations in the jet pedestal," Nucl. Fusion **61**(3), 036015 (2021).

[23]A. Ashourvan, B. A. Grierson, D. J. Battaglia, S. R. Haskey, and T. Stoltzfus-Dueck, "Validation of the kinetic-turbulent-neoclassical theory for edge intrinsic rotation in DIII-D," Phys. Plasmas **25**(5), 056114 (2018).

[24]W. Guttenfelder, J. Candy, S. M. Kaye, W. M. Nevins, E. Wang, R. E. Bell, G. W. Hammett, B. P. LeBlanc, D. R. Mikkelsen, and H. Yuh, "Electromagnetic transport from microtearing mode turbulence," Phys. Rev. Lett. **106**(15), 155004 (2011).

[25]S. Moradi, I. Pusztai, W. Guttenfelder, T. Fülöp, and A. Mollén, "Microtearing modes in spherical and conventional tokamaks," Nucl. Fusion **53**(6), 063025 (2013).

[26]F. M. Laggner, E. Wolfrum, M. Cavedon, F. Mink, E. Viezzer, M. G. Dunne, P. Manz, H. Doerk, G. Birkenmeier, R. Fischer *et al.*, "High frequency magnetic fluctuations correlated with the inter-ELM pedestal evolution in ASDEX upgrade," Plasma Phys. Controlled Fusion **58**(6), 065005 (2016).

[27]A. Diallo, R. J. Groebner, T. L. Rhodes, D. J. Battaglia, D. R. Smith, T. H. Osborne, J. M. Canik, W. Guttenfelder, and P. B. Snyder, "Correlations between quasi-coherent fluctuations and the pedestal evolution during the inter-edge localized modes phase on DIII-D," Phys. Plasmas **22**(5), 056111 (2015).

[28]J. Chen, D. L. Brower, W. X. Ding, Z. Yan, T. Osborne, E. Strait, M. Curie, D. R. Hatch, M. T. Kotschenreuther, X. Jian *et al.*, "Internal measurement of magnetic turbulence in ELMy H-mode tokamak plasmas," Phys. Plasmas **27**(12), 120701 (2020).

[29]J. Chen, D. L. Brower, W. X. Ding, Z. Yan, M. Curie, M. T. Kotschenreuther, T. Osborne, E. Strait, D. R. Hatch, M. R. Halfmoon *et al.*, "Pedestal magnetic turbulence measurements in ELMy H-mode DIII-D plasmas by Faraday-effect polarimetry," Phys. Plasmas **28**(2), 022506 (2021).

[30]D. R. Hatch, M. T. Kotschenreuther, S. M. Mahajan, M. R. Halfmoon, E. Hassan, G. Merlo, C. Michoski, J. Canik, A. C. Sontag, and I. Joseph, "Final report FY19 FES theory performance target," T3chnical Report No. 1615233, 2019.

[31]E. Hassan, D. R. Hatch, M. R. Halfmoon, M. Curie, M. T. Kotchenreuther, S. M. Mahajan, G. Merlo, R. J. Groebner, A. O. Nelson, and A. Diallo, "Identifying the microtearing modes in the pedestal of DIII-D H-modes using gyrokinetic simulations," Nucl. Fusion **62**(2), 026008 (2021).

[32]M. Curie, M. R. Halfmoon, J. Chen, D. R. Hatch, D. L. Brower, E. Hassan, M. T. Kotschenreuther, M. J. Mahajan, and R. J. Groebner, "Gyrokinetic simulations compared with magnetic fluctuations diagnosed with a Faraday-effect radial interferometer-polarimeter in the DIII-D pedestal," (published online).

[33]A. O. Nelson, F. M. Laggner, A. Diallo, D. Smith, A. Xing, R. Shousha, and E. Kolemen, "Time-dependent experimental identification of inter-ELM microtearing modes in the tokamak edge on DIII-D," Nucl. Fusion **61**, 116038 (2021).

[34]D. J. Applegate, C. M. Roach, J. W. Connor, S. C. Cowley, W. Dorland, R. J. Hastie, and N. Joiner, "Micro-tearing modes in the mega ampere spherical tokamak," Plasma Phys. Controlled Fusion **49**(8), 1113 (2007).
[35]H. Doerk, F. Jenko, M. J. Pueschel, and D. R. Hatch, "Gyrokinetic microtearing turbulence," Phys. Rev. Lett. **106**(15), 155003 (2011).
[36]D. R. Hatch, M. J. Pueschel, F. Jenko, W. M. Nevins, P. W. Terry, and H. Doerk, "Origin of magnetic stochasticity and transport in plasma microturbulence," Phys. Rev. Lett. **108**(5), 235002 (2012).
[37]J. C. Hillesheim, D. Dickinson, C. M. Roach, S. Saarelma, R. Scannell, A. Kirk, N. A. Crocker, W. A. Peebles, and H. Meyer, "Intermediate-k density and magnetic field fluctuations during inter-ELM pedestal evolution in MAST," Plasma Phys. Controlled Fusion **58**(1), 014020 (2015).
[38]P. B. Snyder, R. J. Groebner, A. W. Leonard, T. H. Osborne, and H. R. Wilson, "Development and validation of a predictive model for the pedestal height," Phys. Plasmas **16**, 056118 (2009).
[39]T. Goerler, X. Lapillonne, S. Brunner, T. Dannert, F. Jenko, F. Merz, and D. Told, "The global version of the gyrokinetic turbulence code gene," J. Comput. Phys. **230**(18), 7053–7071 (2011).
[40]O. Meneghini, S. P. Smith, L. L. Lao, O. Izacard, Q. Ren, J. M. Park, J. Candy, Z. Wang, C. J. Luna, V. A. Izzo, B. A. Grierson, P. B. Snyder, C. Holland, J. Penna, G. Lu, P. Raum, A. McCubbin, D. M. Orlov, E. A. Belli, N. M. Ferraro, R. Prater, T. H. Osborne, A. D. Turnbull, and G. M. Staebler, "Integrated modeling applications for tokamak experiments with OMFIT," Nucl. Fusion **55**(8), 083008 (2015).
[41]Z. A. Xing, D. Eldon, A. O. Nelson, M. A. Roelofs, W. J. Eggert, O. Izacard, A. S. Glasser, N. C. Logan, O. Meneghini, S. P. Smith *et al.*, "Cake: Consistent automatic kinetic equilibrium reconstruction," Fusion Eng. Des. **163**, 112163 (2021).
[42]A. O. Nelson, F. M. Laggner, R. Groebner, B. A. Grierson, O. Izacard, D. Eldon, M. W. Shafer, A. Leonard, D. Shiraki, A. C. Sontag *et al.*, "Setting the H-mode pedestal structure: Ariations of particle source location using gas puff and pellet fueling," Nucl. Fusion **60**(4), 046003 (2020).
[43]F. W. Perkins and J. H. Doles III, "Velocity shear and the E × B instability," J. Geophys. Res. **80**(1), 211–214, https://doi.org/10.1029/JA080i001p00211 (1975).
[44]A. M. Dimits, G. Bateman, M. A. Beer, B. I. Cohen, W. Dorland, G. W. Hammett, C. Kim, J. E. Kinsey, M. T. Kotschenreuther, A. H. Kritz *et al.*, "Comparisons and physics basis of tokamak transport models and turbulence simulations," Phys. Plasmas **7**(3), 969–983 (2000).
[45]D. R. Hatch, M. J. Pueschel, F. Jenko, F. W. Nevins, P. W. Terry, and H. Doerk, "Magnetic stochasticity and transport due to nonlinearly excited subdominant microtearing modes," Phys. Plasmas **20**(1), 012307 (2013).
[46]A. B. Navarro, T. Happel, T. Görler, F. Jenko, J. Abiteboul, A. Bustos, H. Doerk, D. Told, and ASDEX Upgrade Team, "Gyrokinetic studies of core turbulence features in ASDEX upgrade H-mode plasmas," Phys. Plasmas **22**(4), 042513 (2015).
[47]X. Garbet, Y. Idomura, L. Villard, and T. H. Watanabe, "Gyrokinetic simulations of turbulent transport," Nucl. Fusion **50**(4), 043002 (2010).
[48]M. R. Fahey and J. Candy, "Gyro: A 5D gyrokinetic-Maxwell solver," in *SC'04: Proceedings of the 2004 ACM/IEEE Conference on Supercomputing* (IEEE, 2004), p. 26.
[49]J. Chowdhury, S. H. Ku, J. Dominski, R. Hager, D. Mikkelsen, W. Guttenfelder, P. Porazik, and C. S. Chang, "Gyrokinetic study of electron transport in NSTX using XGC," APS Div. Plasma Phys. Meet. Abstr. **2017**, PP11–051. Available at https://ui.adsabs.harvard.edu/abs/2017APS..DPPP11051C/abstract
[50]N. Howard, C. Holland, A. White, M. Reinke, T. Rhodes, M. Greenwald, J. Candy, and Alcator C-Mod Team, "The effect of ITG/TEM mix on gyrokinetic modeling of an Alcator C-Mod current scan," APS Div. Plasma Phys. Meet. Abstr. **2013**, CO4–006.
[51]C. Holland, T. C. Luce, B. A. Grierson, S. P. Smith, A. Marinoni, K. H. Burrell, C. C. Petty, and E. M. Bass, "Examination of stiff ion temperature gradient mode physics in simulations of DIII-D H-mode transport," Nucl. Fusion **61**(6), 066033 (2021).
[52]A. E. White, L. Schmitz, G. R. McKee, C. Holland, W. A. Peebles, T. A. Carter, M. W. Shafer, M. E. Austin, K. H. Burrell, J. Candy *et al.*, "Measurements of core electron temperature and density fluctuations in DIII-D and comparison to nonlinear gyrokinetic simulations," Phys. Plasmas **15**(5), 056116 (2008).
[53]D. R. Ernst, K. H. Burrell, W. Guttenfelder, T. L. Rhodes, A. M. Dimits, R. Bravenec, B. A. Grierson, C. Holland, J. Lohr, A. Marinoni, G. R. McKee, C. C. Petty, J. C. Rost, L. Schmitz, G. Wang, S. Zemedkun, and L. Zeng, "Role of density gradient driven trapped electron mode turbulence in the H-mode inner core with electron heating," Phys. Plasmas **23**(5), 056112 (2016).
[54]R. M. Churchill, C. S. Chang, S. Ku, and J. Dominski, "Pedestal and edge electrostatic turbulence characteristics from an XGC1 gyrokinetic simulation," Plasma Phys. Controlled Fusion **59**(10), 105014 (2017).
[55]X. Liu, "Gyrokinetic simulation of pedestal turbulence using GENE," Ph.D. thesis (University of Texas at Austin, 2018).
[56]J. L. Larakers, M. Curie, D. R. Hatch, R. D. Hazeltine, and S. M. Mahajan, "Global theory of microtearing modes in the tokamak pedestal," Phys. Rev. Lett. **126**(22), 225001 (2021).
[57]D. Jarema, H. J. Bungartz, T. Görler, F. Jenko, T. Neckel, and D. Told, "Block-structured grids for Eulerian gyrokinetic simulations," Comput. Phys. Commun. **198**, 105–117 (2016).
[58]D. Jarema, H. J. Bungartz, T. Görler, F. Jenko, T. Neckel, and D. Told, "Block-structured grids in full velocity space for Eulerian gyrokinetic simulations," Comput. Phys. Commun. **215**, 49–62 (2017).
[59]M. T. Curie, J. L. Larakers, D. R. Hatch, A. O. Nelson, A. Diallo, E. Hassan, W. Guttenfelder, M. Halfmoon, M. Kotschenreuther, R. D. Hazeltine, S. M. Mahajan, R. J. Groebner, J. Chen, C. Perez von Thun, L. Frassinetti, S. Saarelma, C. Giroud, and M. M. Tennery, "A survey of pedestal magnetic fluctuations using gyrokinetics and a global reduced model for microtearing stability," Phys. Plasmas **29**(4), 042503 (2022).
[60]I. Predebon and F. Sattin, "On the linear stability of collisionless microtearing modes," Phys. Plasmas **20**(4), 040701 (2013).
[61]M. Hamed, M. Muraglia, Y. Camenen, and X. Garbet, "Stability of a slab collisional microtearing mode," Contrib. Plasma Phys. **58**(6-8), 529–533 (2018).
[62]L. F. Drake and Y. C. Lee, "Kinetic theory of tearing instabilities," Phys. Fluids **20**(8), 1341–1353 (1977).
[63]E. A. Belli and J. Candy, "Kinetic calculation of neoclassical transport including self-consistent electron and impurity dynamics," Plasma Phys. Controlled Fusion **50**(9), 095010 (2008).
[64]E. A. Belli and J. Candy, "Full linearized Fokker–Planck collisions in neoclassical transport simulations," Plasma Phys. Controlled Fusion **54**(1), 015015 (2011).
[65]M. J. Pueschel, M. Kammerer, and F. Jenko, "Gyrokinetic turbulence simulations at high plasma beta," Phys. Plasmas **15**(10), 102310 (2008).
[66]J. R. King, S. E. Kruger, K. H. Burrell, X. Chen, A. M. Garofalo, R. J. Groebner, K. E. J. Olofsson, A. Y. Pankin, and P. B. Snyder, "MHD modeling of a DIII-D low-torque QH-mode discharge and comparison to observations," Phys. Plasmas **24**(5), 055902 (2017).
[67]G. W. Hammett, W. Dorland, and F. W. Perkins, "Fluid models of phase mixing, Landau damping, and nonlinear gyrokinetic dynamics," Phys. Fluids B: Plasma Phys. **4**(7), 2052–2061 (1992).
[68]C. H. Ma and X. Q. Xu, "Global kinetic ballooning mode simulations in Bout++," Nucl. Fusion **57**(1), 016002 (2016).
[69]C. F. Figarella, S. Benkadda, P. Beyer, X. Garbet, and I. Voitsekhovitch, "Transport reduction by rotation shear in tokamak-edge turbulence," Phys. Rev. Lett. **90**, 015002 (2003).